\



Evolution of superconductivity and charge order inpressurized RbV_3Sb_5

Feng Du(杜锋), Shuaishuai Luo(罗帅帅), Rui Li(李蕊), Brenden R. Ortiz, Ye Chen(陈晔),Stephen D. Wilson, Yu Song(宋宇), and Huiqiu Yuan(袁辉球)

Citation: Chin. Phys. B, 2022, 31 (**1**): 017404. DOI: 10.1088/1674-1056/ac4232
Journal homepage: http://cpb.iphy.ac.cn; http://iopscience.iop.org/cpb

What follows is a list of articles you may be interested in

Pressure tuning of the anomalous Hall effect in the kagome superconductor CsV_3Sb_5

Fang-Hang Yu(喻芳航), Xi-Kai Wen(温茜凯), Zhi-Gang Gui(桂智刚), Tao Wu(吴涛), Zhenyu Wang(王震宇), Zi-Ji Xiang(项子雾), Jianjun Ying(应剑俊), and Xianhui Chen(陈仙辉)

Chin. Phys. B, 2022, 31 (**1**): 017405. DOI: 10.1088/1674-1056/ac3990

Temperature and doping dependent flat-band superconductivity on the Lieb-lattice

Feng Xu(徐峰), Lei Zhang(张磊), and Li-Yun Jiang(姜立运)

Chin. Phys. B, 2021, 30 (**6**): 067401. DOI: 10.1088/1674-1056/abdea5

Physical properties and phase diagram of $NaFe_{1-x}V_xAs$

Guang-Yang Dai(代光阳), Xin He(何鑫), Zhi-Wen Li(李芷文), Chang-Ling Zhang(张昌玲), Lu-Chuan Shi(史鲁川), Run-Ze Yu(于润泽), Xian-Cheng Wang(望贤成), and Chang-Qing Jin(靳常青)

Chin. Phys. B, 2021, 30 (**1**): 017401. DOI: 10.1088/1674-1056/abcf95

Cubic anvil cell apparatus for high-pressure and low-temperature physical property measurements

Jin-Guang Cheng(程金光), Bo-Sen Wang(王铂森), Jian-Ping Sun(孙建平), Yoshiya Uwatoko

Chin. Phys. B, 2018, 27 (**7**): 077403. DOI: 10.1088/1674-1056/27/7/077403

Multiband nodeless superconductivity near the charge-density-wave quantum critical point in $ZrTe_{3-x}Se_x$

Shan Cui(崔珊), Lan-Po He(何兰坡), Xiao-Chen Hong(洪晓晨), Xiang-De Zhu(朱相德), Cedomir Petrovic, Shi-Yan Li(李世燕)

Chin. Phys. B, 2016, 25 (**7**): 077403. DOI: 10.1088/1674-1056/25/7/077403

SPECIAL TOPIC — Superconductivity in vanadium-based kagome materials

Evolution of superconductivity and charge order in pressurized RbV_3Sb_5

Feng Du(杜锋)[1,2], Shuaishuai Luo(罗帅帅)[1,2], Rui Li(李蕊)[1,2], Brenden R. Ortiz[3], Ye Chen(陈晔)[1,2], Stephen D. Wilson[3], Yu Song(宋宇)[1,2,†], and Huiqiu Yuan(袁辉球)[1,2,4,‡]

[1] *Center for Correlated Matter and Department of Physics, Zhejiang University, Hangzhou* 310058, *China*
[2] *Zhejiang Province Key Laboratory of Quantum Technology and Device, Department of Physics, Zhejiang University, Hangzhou* 310058, *China*
[3] *Materials Department and California Nanosystems Institute, University of California Santa Barbara, Santa Barbara, CA* 93106, *United States*
[4] *State Key Laboratory of Silicon Materials, Zhejiang University, Hangzhou* 310058, *China*

(Received 21 August 2021; revised manuscript received 29 November 2021; accepted manuscript online 11 December 2021)

The kagome metals AV_3Sb_5 (A = K, Rb, Cs) under ambient pressure exhibit an unusual charge order, from which superconductivity emerges. In this work, by applying hydrostatic pressure using a liquid pressure medium and carrying out electrical resistance measurements for RbV_3Sb_5, we find that the charge order becomes suppressed under a modest pressure p_c (1.4 GPa$< p_c <$ 1.6 GPa), while the superconducting transition temperature T_c is maximized. T_c is then gradually weakened with further increase of pressure and reaches a minimum around 14.3 GPa, before exhibiting another maximum around 22.8 GPa, signifying the presence of a second superconducting dome. Distinct normal state resistance anomalies are found to be associated with the second superconducting dome, similar to KV_3Sb_5. Our findings point to qualitatively similar temperature–pressure phase diagrams in KV_3Sb_5 and RbV_3Sb_5, and suggest a close link between the second superconducting dome and the high-pressure resistance anomalies.

Keywords: kagome superconductor, temperature–pressure phase diagram, superconducting dome, hydrostatic pressure

PACS: 74.25.Dw, 74.62.Fj, 74.25.F−

DOI: 10.1088/1674-1056/ac4232

1. Introduction

The kagome metals AV_3Sb_5 (A = K, Rb, Cs)[1–4] have drawn significant interest recently, with focus on (1) superconductivity with topological surfaces states,[2] which raises the prospects of realizing topological superconductivity and Majorana zero modes;[5,6] (2) a large anomalous Hall effect in the absence of local moments,[7–9] which possibly results from a charge order that breaks time-reversal symmetry;[10–13] (3) the nature of the superconducting pairing, with evidence for nodeless superconducting gaps,[14–16] as well as indications for nematic superconductivity;[17] and (4) the sensitivity of superconductivity and charge order to pressure-tuning,[18–26] likely related to the presence of competing instabilities on the kagome lattice.[27–31]

With the application of pressure, the charge order becomes quickly suppressed and superconductivity is enhanced, forming a superconducting dome with maximal T_c near the pressure at which the charge order disappears.[18–24,26] While this superconducting dome can be understood to result from the competition between superconductivity and charge order, a second superconducting dome is found in AV_3Sb_5 at higher pressures,[18,21–24] whose origin remains unclear. Factors that may be relevant for the formation of the second superconducting dome include a pressure-induced Lifshitz transition,[22] magnetism suppressing superconductivity in the region between the two superconducting domes,[32] reconstruction of the Sb bands due to the formation of interlayer Sb–Sb bonds,[33] and a distinct high-pressure phase revealed through resistivity anomalies.[21] While two-dome superconductivity is found in all AV_3Sb_5 materials via resistivity measurements,[24] studies of the corresponding normal state from which superconductivity emerges has been limited.[21,22] In particular, it remains unclear whether resistivity anomalies associated with the second superconducting dome in KV_3Sb_5[21] are also present in RbV_3Sb_5 and CsV_3Sb_5.

In addition, single crystal diffraction revealed a highly anisotropic compression under hydrostatic pressure, with the c lattice parameter reducing significantly more than the in-plane lattice parameters,[33] which suggests hydrostaticity of measurements under pressure may strongly affect experimental results and the determined phase diagrams. Therefore, to compare results on the AV_3Sb_5 series obtained using different experimental techniques, it is important to reproduce the corresponding experimental hydrostaticity.

In this work, we systematically investigated the temperature–pressure phase diagram of RbV_3Sb_5 via mea-

†Corresponding author. E-mail: yusong_phys@zju.edu.cn
‡Corresponding author. E-mail: hqyuan@zju.edu.cn

© 2022 Chinese Physical Society and IOP Publishing Ltd

surements of electrical resistance, applying pressure using a liquid pressure medium. It is found that the superconducting transition temperature T_c in RbV_3Sb_5 increases from 0.9 K under ambient pressure to about 4.5 K at 1.2 GPa, with the charge order disappearing above p_c, which occurs between 1.4 GPa and 1.6 GPa. T_c is then gradually suppressed with increasing pressure and reaches a minimum of about 0.4 K around 14.3 GPa. With further increase of pressure, another T_c maximum of about 1.2 K is observed around 22.8 GPa, indicating the presence of a second superconducting dome. For pressures $\gtrsim$ 22.8 GPa, T_c in the second superconducting dome is suppressed with increasing pressure, and distinct features are detected in the normal state resistance, possibly related to a high-pressure phase. These behaviors are similar to pressurized KV_3Sb_5,[21] suggesting that they are common in the AV_3Sb_5 series under high pressure, and are closely related to the suppression of superconductivity in the second dome.

2. Experimental details

Single crystals of RbV_3Sb_5 were grown using a self-flux method.[1,2] Electrical resistance measurements under pressure were carried out using a diamond anvil cell (DAC), with silicon oil as the pressure medium, which allows for better hydrostaticity compared to solid pressure media. Single crystals of RbV_3Sb_5 were polished and cut into square pieces, and then loaded into a Be–Cu diamond anvil cell with a 400-μm-diameter culet. The ruby fluorescence method was used to determine the values of pressure inside the DAC at room temperature, before and after the measurements. All electrical resistance measurements from room temperature down to 0.3 K were performed in a Teslatron-PT system with an Oxford ^{3}He insert. For measurements with an applied magnetic field, the field was applied along the c-axis.

3. Results

The measured electrical resistance $R(T)$ for sample #1 with pressures from 0.9 GPa up to 34.2 GPa is shown in Figs. 1(a)–1(d), with the corresponding dR/dT curves shown in Figs. 1(e)–1(g). Examining the behavior of $R(T)$ in the normal state, clear anomalies associated with the charge ordering temperature T_{CO} can be seen up to 1.4 GPa, with T_{CO} decreasing with increasing pressure [Fig. 1(a)]. The values of T_{CO} can be determined from the anomaly in the dR/dT curves, as shown in Fig. 1(e), which becomes indiscernible at 1.6 GPa. These results suggest that the charge order disappears at a critical pressure p_c between 1.4 GPa and 1.6 GPa. p_c in RbV_3Sb_5 is larger than that in KV_3Sb_5 ($\approx$ 0.5 GPa),[21] consistent with the idea that larger alkaline metal ions exert negative chemical pressure, although it should be noted that additional effects may also be at play, as suggested by the complex evolution of T_c with pressure in CsV_3Sb_5 and RbV_3Sb_5 for $p < p_c$.[19,20,26]

In the pressure range from 2.6 GPa to 8.9 GPa, $R(T)$ in the normal state is largely unchanged with increasing pressure [Fig. 1(b)]. In contrast, in the pressure range from 11.5 GPa to 27.8 GPa, the values of $R(T)$ increase with increasing pressure, with the increase particularly prominent for $p \gtrsim$ 22.8 GPa [Fig. 1(c)]. This difference between the results in Figs. 1(b) and 1(c) is largely due to the residual resistance R_0, which is the value of $R(T)$ just before the onset of superconductivity. On the other hand, the variation of $R(T)$ with temperature, which can be captured by $\delta R = R(300\ \mathrm{K}) - R_0$,

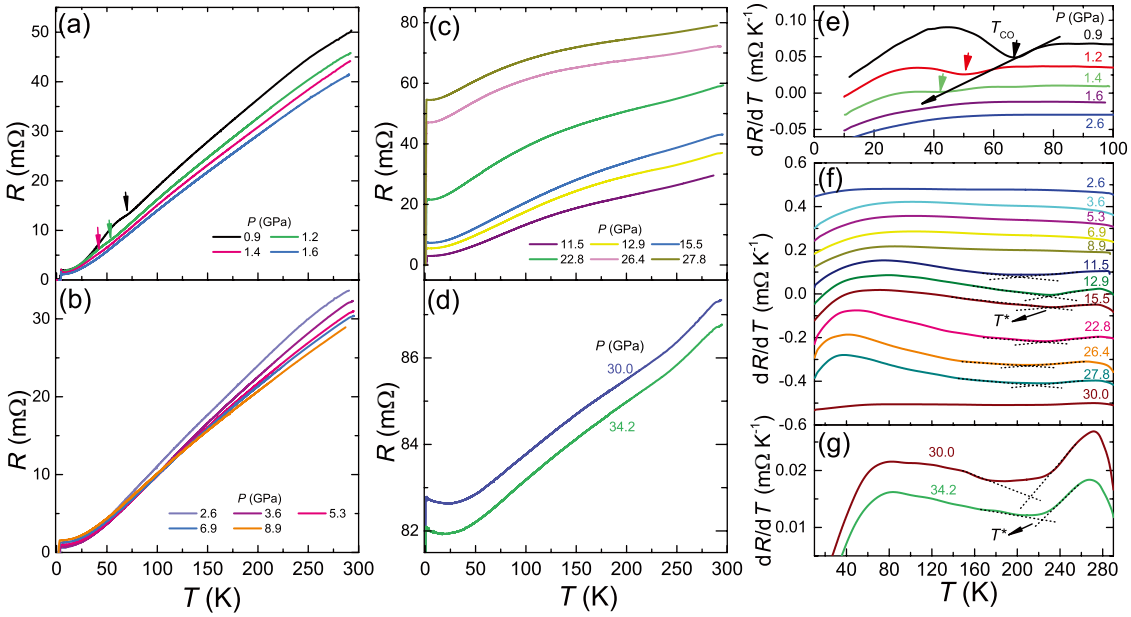


Fig. 1. (a)–(d) Electrical resistance $R(T)$ of RbV_3Sb_5 sample #1 in various pressure ranges. (e)–(g) The corresponding dR/dT curves, shifted vertically for clarity. T_{CO} is the onset temperature of the charge order, and T^* corresponds to a minimum in dR/dT.

stays nearly unchanged from 2.6 GPa to 22.8 GPa, but starts to decrease dramatically when $p \gtrsim 22.8$ GPa. Clear anomalies in $\mathrm{d}R/\mathrm{d}T$, with a minimum at $T^* \sim 220$ K [Figs. 1(f) and 1(b)], are detected for $p \gtrsim 11.5$ GPa. It should be noted that since $\mathrm{d}R/\mathrm{d}T$ exhibits multiple anomalies around T^*, with possible additional features above room temperature, T^* should be considered as a characteristic temperature rather than a transition temperature.

For even higher pressures of 30.0 GPa and 34.2 GPa, the normal state $R(T)$ becomes qualitatively different: compared to lower pressure values, δR is much smaller, R_0 becomes much larger [Fig. 1(d)], and a subtle upturn in $R(T)$ is observed for $T \lesssim 20$ K. In addition, the $\mathrm{d}R/\mathrm{d}T$ anomaly associated with T^* becomes more dominant for $p \gtrsim 30.0$ GPa, due to the dramatic decrease of δR (and thus the magnitude of $\mathrm{d}R/\mathrm{d}T$) at these pressures. These behaviors are similar to KV_3Sb_5 at high pressures,[21] and can be collectively attributed to the formation of a high-pressure phase.

Since the high-pressure phase exhibits a small δR and a large R_0, the observation that δR begins to drop while R_0 begins to increase for $p \gtrsim 22.8$ GPa suggests that the high-pressure phase onsets around 22.8 GPa. On the other hand, signatures of T^* already appear for 11.5 GPa, a significantly lower pressure compared to that when δR begins to drop and R_0 begins to increase, suggesting that is not unique to the high-pressure phase. More work is needed to definitively pin down the phase boundary of the high-pressure phase in the temperature–pressure phase diagram and elucidate the origin of the resistance anomalies around T^*.

Figure 2 zooms into low temperatures to examine the evolution of superconductivity in RbV_3Sb_5 sample #1, as a function of the applied pressure. For pressures from 0.9 GPa to 2.6 GPa [Fig. 2(a)], T_c is bunched around 4 K, significantly higher than $T_c < 1$ K under ambient pressure.[3] A prominent feature is that the superconducting transition is significantly broader for 0.9 GPa, compared to those from 1.2 GPa to 2.6 GPa, which suggests that a broad superconducting transition is correlated with the presence of a strong charge order. It should be noted that while signatures of the charge order are also detected for 1.2 GPa and 1.4 GPa, the corresponding dip in $\mathrm{d}R/\mathrm{d}T$ is significantly weakened compared to that at 0.9 GPa, which indicates that the magnitude of the charge order parameter becomes significantly reduced. A similar sharpening of the superconducting transition with weakening of the charge order upon applying pressure is also observed in KV_3Sb_5,[21] suggesting that it is a common feature of the AV_3Sb_5 series.

One possible origin for this behavior is that $\mathrm{d}T_c/\mathrm{d}p$ is much larger in the presence of a strong charge order, compared to that when the charge order is significantly weakened or suppressed. If there is a distribution of internal stress Δp in the sample (and assume that it does not change too much with applied pressure), then the superconducting transition width $\Delta T_c \approx \frac{\mathrm{d}T_c}{\mathrm{d}p}\Delta p$ would be large when $\mathrm{d}T_c/\mathrm{d}p$ is large.

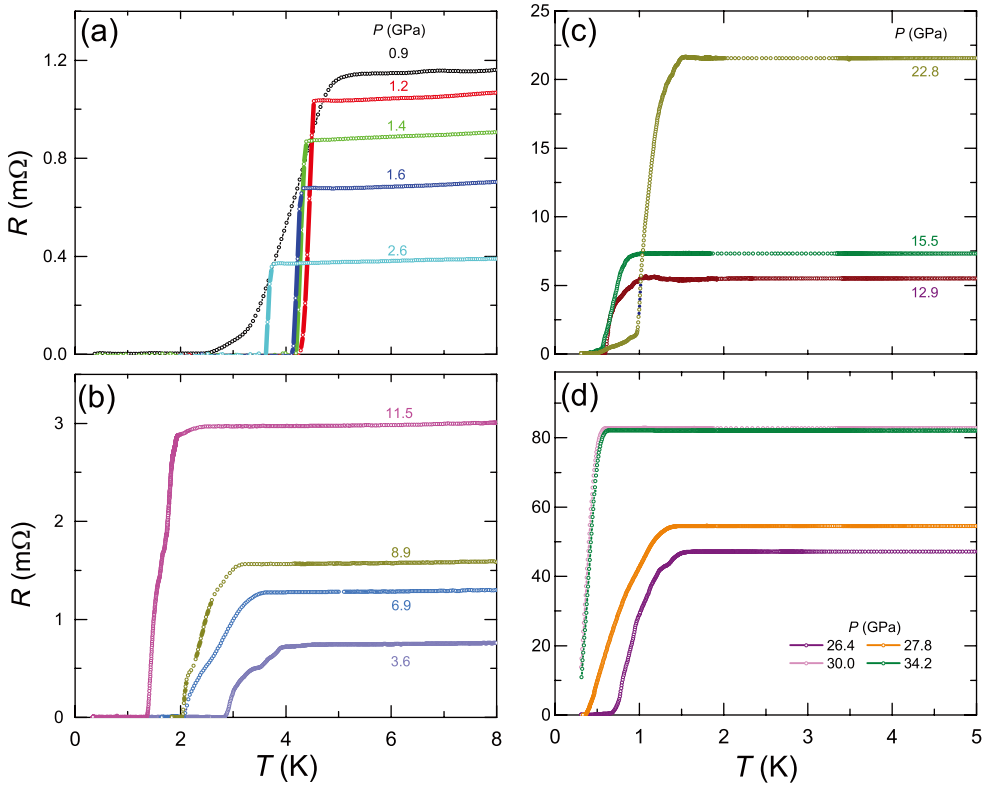


Fig. 2. Zoomed-in electrical resistance $R(T)$ of RbV_3Sb_5 sample #1 under various pressures to show the evolution of superconductivity with pressure.

Alternatively, domain boundaries of a period-2 charge order could exhibit enhanced filamentary superconductivity, leading to a broad superconducting transition in $R(T)$. Such a picture was invoked to account for enhanced superconductivity seen in the period-2 charge order phase of $Ba_{1-x}Sr_xNi_2As_2$, while such an effect was absent for the period-3 charge order phase in the same material series.[34] Given the charge order in AV_3Sb_5 is period-2 in the *ab*-plane,[2] such a mechanism may also contribute to its broadened superconducting transition under ambient and low pressures, where the charge order is substantial.

In the pressure range from 3.6 GPa to 11.5 GPa [Fig. 2(b)], T_c gradually reduces with increasing pressure, which in combination with results in Fig. 2(a), evidences a superconducting dome with maximal T_c around p_c. Such a behavior was previously reported for the AV_3Sb_5 materials,[18–21,24] and likely results from a competition between charge order and superconductivity, without a prominent role of quantum criticality.[21]

Upon further increasing pressure, T_c further drops for 12.9 GPa and 15.5 GPa, but becomes enhanced again at 22.8 GPa [Fig. 2(c)]. This suggests the presence of a minimum in T_c between 12.9 GPa and 22.8 GPa, and signifies the appearance of a second superconducting dome. For pressures in the range from 26.4 GPa to 34.2 GPa [Fig. 2(d)], T_c decreases with increasing pressure, indicating that the maximal T_c of the second superconducting dome appears at $p < 26.4$ GPa. Moreover, the superconducting transition becomes sharpened for 30.0 GPa and 34.2 GPa, possibly related to the high-pressure phase, with clear signatures in the normal state. It is interesting to note that the suppression of superconductivity in RbV_3Sb_5 is less significant compared to that in KV_3Sb_5, as the high-pressure phase appears. Compared to superconducting transitions for $p \leq 2.6$ GPa, those for $p \geq 3.6$ GPa are generally broader and less smooth, possibly related to a larger distribution of stress or pressure-induced defects in the crystal.

To clarify the evolution of T_c near the boundary of the two superconducting domes, we measured $R(T)$ near T_c for RbV_3Sb_5 sample #2, with results shown in Fig. 3. Upon increasing pressure from 1.8 GPa up to 14.3 GPa [Fig. 3(a)], T_c monotonically decreases with increasing pressure, with the value of T_c (determined through the midpoint of the superconducting transition) reaching a minimum of about 0.4 K at 14.3 GPa. With further increase of pressure, T_c becomes slightly enhanced at 15.1 GPa, and furthers increases with increasing pressure up to 21.6 GPa [Fig. 3]. Upon further increase of pressure, T_c again reduces with increasing pressure [Fig. 3]. These measurements on sample #2 are consistent with those for sample #1 [Fig. 2] in establishing the presence of two superconducting domes, and further clarifies that the minimum in T_c between the two domes occurs around 14.3 GPa.

To probe the superconducting state under various pressures, we chose three representative pressures and measured the resistance for sample #1 under an applied magnetic field along the *c*-axis, with results shown in Fig. 4. The three pressures correspond to states with coexisting charge order and superconductivity [0.9 GPa, Fig. 4(a)], without charge order and inside the first superconducting dome [2.6 GPa, Fig. 4(b)], and inside the second superconducting dome [27.8 GPa, Fig. 4(c)]. As can be seen, superconductivity is gradually suppressed with applied field in all cases, which allows us to extract the upper critical field $\mu_0 H_{c2}(T)$ for various pressures.

The upper critical fields $\mu_0 H_{c2}(T)$ are determined as when $R(T)$ drops to $R_0/2$, and are summarized in Fig. 4(d). $\mu_0 H_{c2}(T)$ could be fit with the Werthamer–Helfand–Hohenberg (WHH) model[35] for the three pressures, with fits shown as dashed lines in Fig. 4(d). Previously, it was shown in KV_3Sb_5 that a much larger $\mu_0 H_{c2}(T=0)$ (for field along the *c*-axis) is observed for the second superconducting dome, even when the T_c is lower compared to the first superconducting dome.[21] For RbV_3Sb_5, the values of $T_c^2/\mu_0 H_{c2}(T=0)$ are respectively found to be 13.3, 15.2 and 1.9 (K^2/T), for 0.9 GPa, 2.6 GPa and 27.8 GPa. The significantly smaller ratio at 27.8 GPa points to $\mu_0 H_{c2}(T=0)$ also becoming enhanced relative to T_c in the second superconducting dome, similar to KV_3Sb_5.

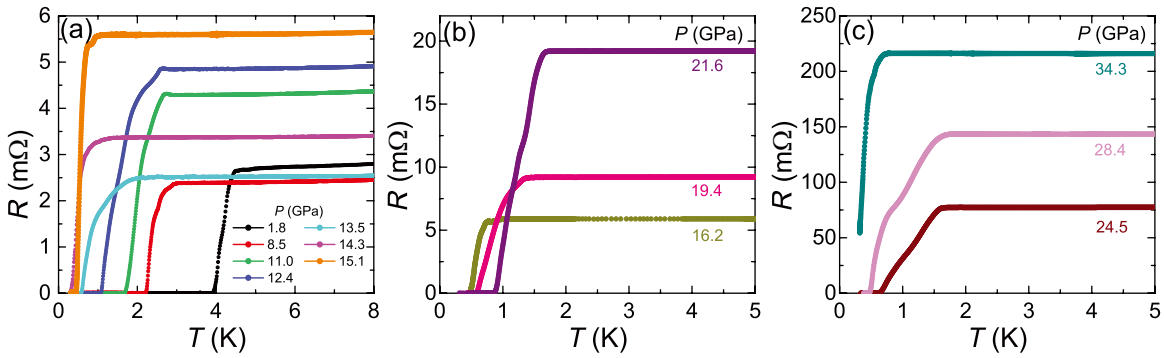


Fig. 3. Electrical resistance $R(T)$ of RbV_3Sb_5 sample #2 near the superconducting transition under various pressures, showing the evolution of superconductivity with pressure.

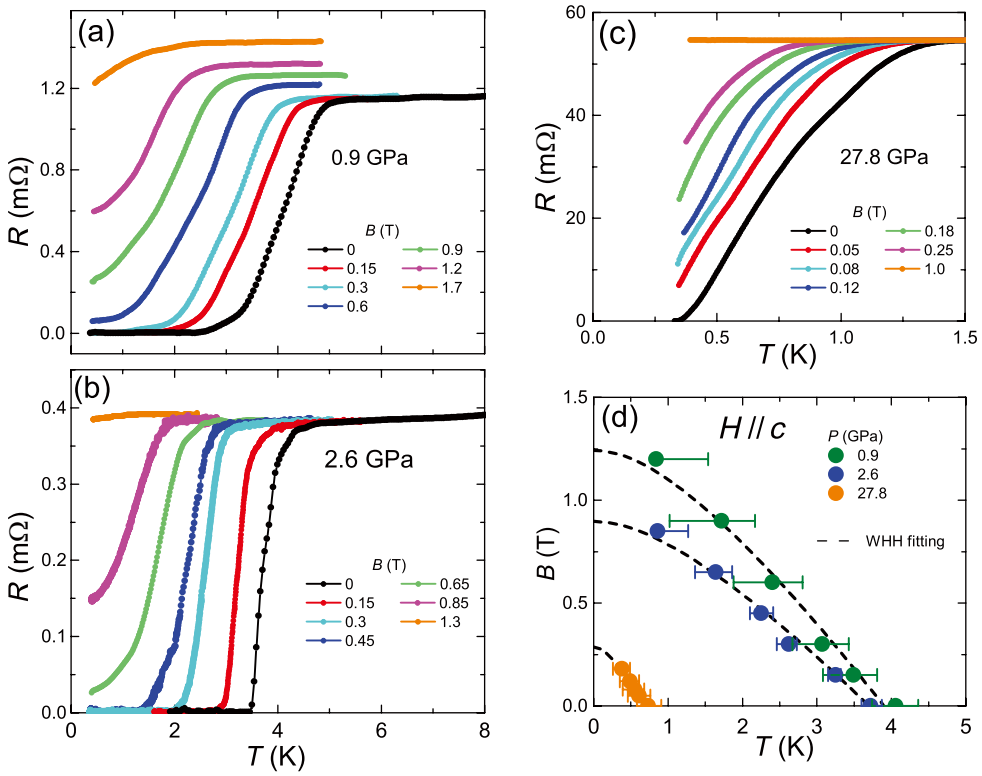


Fig. 4. Low-temperature electrical resistance $R(T)$ of RbV_3Sb_5 sample #1 under various c-axis magnetic fields, for applied pressures (a) 0.9 GPa, (b) 2.6 GPa, and (c) 27.8 GPa. (d) The upper critical fields of RbV_3Sb_5, as a function of temperature under pressures of 0.9 GPa, 2.6 GPa, and 27.8 GPa. Fits to the WHH model are shown as dashed lines.

The phase diagram obtained from electrical resistance measurements under pressure is shown in Fig. 5(a). T_c is determined as when $R(T)$ drops to $R_0/2$, T^* from a minimum in dR/dT [Fig. 1(g)], and T_{CO} from the dip in dR/dT [Fig. 1(e)]. In KV_3Sb_5, it was shown that the decrease of T_c above p_c is much more gradual, compared to the enhancement of T_c below p_c, resulting in the first superconducting dome being highly asymmetric.[21] In the case of RbV_3Sb_5, it can be seen that the same qualitative behavior is observed.

Various regimes in the phase diagram can be identified through the presence of a resistivity anomaly at T^* [Fig. 5(a)] and signatures in δR and R_0 [Fig. 5(b)]. The anomaly in dR/dT associated with T^* first appears at 11.5 GPa, just before superconductivity crossovers from the first dome into the second. R_0 increases slowly with increasing pressure up to ~ 22.8 GPa, above which it increases at a much faster rate up to ~ 30 GPa, and finally plateaus for $p \gtrsim 30$ GPa. δR exhibits a gradual decrease with increasing pressure up to 1.4 GPa ($\approx p_c$), then evolves slowly up to ~ 22.8 GPa, before dropping precipitously for $p \gtrsim 22.8$ GPa. Since T_c in the second superconducting dome begins to decrease with increasing pressure for $p \gtrsim 22.8$ GPa, a large R_0 and a small δR, which are signatures of a possible high-pressure phase, appear to be correlated with suppression of T_c in the second superconducting dome. A similar large drop of δR and an increase in R_0 are also observed in KV_3Sb_5, and are also associated with the suppression of T_c in the second superconducting dome.[21]

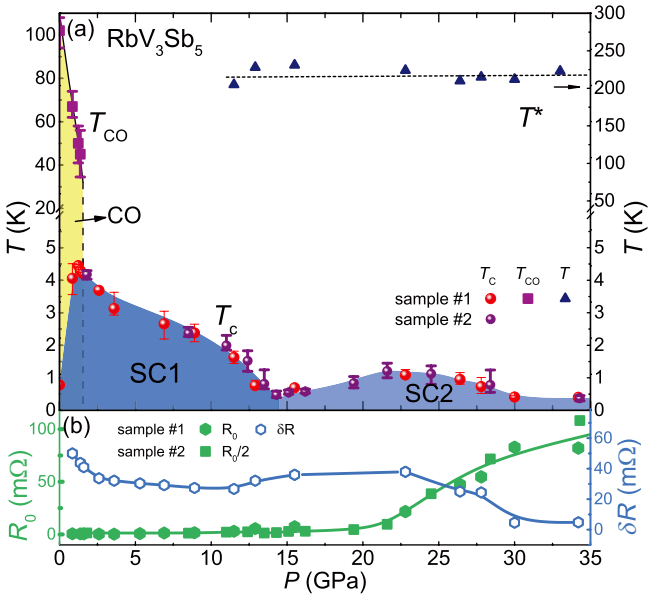


Fig. 5. (a) The temperature–pressure phase diagram of RbV_3Sb_5. Two superconducting regions (SC1 and SC2) and a charge-ordered phase (CO) are identified. Points under ambient pressure are from Ref. [3]. T_{CO} is the onset temperature of the charge order, T_c is the superconducting transition temperature, and T^* is a characteristic temperature associated with a minimum in dR/dT. The errors bars for T_{CO} are determined from the half width at half minimum of the dip in dR/dT. The errors bars for T_c characterize the width of the superconducting transition, with values corresponding to 20% and 80% of R_0, where R_0 is the resistance just before the onset of superconductivity. In cases where $R(T)$ does not drop to 20% of R_0 at the lowest measured temperature, $R(T)$ is extrapolated to obtain an estimate. (b) Pressure dependence of the residual resistance R_0 and the electrical resistance change $\delta R = R(300\ \mathrm{K}) - R_0$. R_0 for sample #2 is divided by 2, and plotted together with R_0 for sample #1. δR was only measured for sample #1. The solid lines are guides-to-the-eyes.

4. Discussion and conclusion

Our observation of two-dome superconductivity is similar to previous works on AV_3Sb_5,[18,21–24] and suggests that such a feature is qualitatively robust, both with regard to variations of the alkaline metal and experimental hydrostaticity. On the other hand, the additional modulation of T_c for $p < p_c$ in CsV_3Sb_5 and RbV_3Sb_5[19,20,26] is not observed in KV_3Sb_5.[21] While the present data on RbV_3Sb_5 suggests a single peak in T_c around p_c, the density of probed pressures is insufficient to distinguish whether additional subtle modulations of T_c exist for $p < p_c$.[26]

Despite the qualitative agreement on the presence of two-dome superconductivity in the literature, directly comparing phase diagrams for RbV_3Sb_5 from this work and Ref. [24] [Fig. 6(a)], and for KV_3Sb_5 from Refs. [21,24] [Fig. 6(b)], reveals clear differences. The differences likely originate from hydrostaticity of the experiments, which either used silicon oil as a liquid pressure medium (solid symbols, this work and Ref. [21]), or cubic boron nitride as a solid pressure medium (open symbols, Ref. [24]), with the former typically associated with better hydrostatcity. As can be seen, in the phase diagrams of both RbV_3Sb_5 and KV_3Sb_5 obtained using a liquid pressure medium, a larger pressure is required to suppress the first superconducting dome (and induce the onset of the second dome), compared to experiments using a solid pressure medium. On the other hand, superconductivity in the second dome appears more easily suppressed using a liquid medium, while it is more persistent when using a solid medium. While the origin for these systematic differences remains unclear, a key factor is the strongly anisotropic compression revealed under pressure, with the c-axis lattice parameter reduced by a staggering $\sim 20\%$ under 20 GPa in CsV_3Sb_5.[33] Since typical studies on layered materials in a DAC apply force along the c-axis, nonideal hydrostaticity could lead to larger-than-nominal compressive pressure on the ab-plane. This may contribute to the smaller nominal pressures in experiments using a solid pressure medium, which are needed to access, for example, the dip in T_c between the two superconducting domes. These observations point to the importance of hydrostaticity for experimentally determined phase diagrams, which should be taken into consideration when comparing experimental results on AV_3Sb_5 obtained under high-pressures.

Comparing the present results on RbV_3Sb_5 with previous work on KV_3Sb_5[21] [solid symbols in Figs. 6(a) and 6(b)], it can be seen a higher suppress of the first superconducting dome in RbV_3Sb_5, consistent with the notion that a larger atomic radius corresponds to negative chemical pressure. More importantly, clear changes in the normal state transport (R_0 and δR), which can be attributed to a high-pressure phase, are seen under pressures associated with the suppression of T_c in the second superconducting dome, for both RbV_3Sb_5 and KV_3Sb_5.[21] With increasing pressure, the dR/dT anomaly near T^* first appears at the edge of the first superconducting dome, and persists across the second superconducting dome. Previous work on KV_3Sb_5[21] also associated the resistance anomalies around T^* with the high-pressure phase and the suppression of T_c in the second superconducting dome. Examination of the published data reveals that these anomalies in KV_3Sb_5 also extend to lower pressures, suggesting that they are not unique to the high-pressure phase, similar to the present results on RbV_3Sb_5.

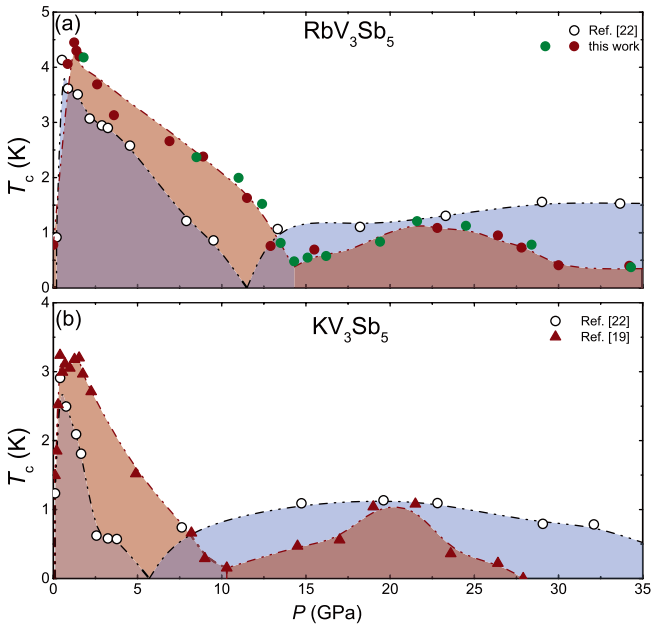


Fig. 6. (a) Comparison between superconducting phase diagrams of RbV_3Sb_5 from this work and Ref. [24]. The maroon symbols are from RbV_3Sb_5 sample #1, and the green symbols are from sample #2. (b) Comparison between superconducting phase diagrams of KV_3Sb_5 from Refs. [21,24]. T_c in this work and Ref. [21] is defined as when the resistance (resistivity) drops to $R_0/2$ ($\rho_0/2$), whereas it is determined from $0.9\rho_0$ in Ref. [24]. The dashed lines are guides-to-the-eyes.

It is interesting to note that for pressures associated with the second superconducting dome in CsV_3Sb_5, Raman spectroscopy detected distinct signatures in the phonon spectrum,[22] and first-principles calculations found a structural instability[32] and a reconstruction of the Fermi surface,[33] suggesting that the normal state from which superconductivity emerges in the second dome of CsV_3Sb_5 is distinct from that at lower pressures, similar to the present findings for RbV_3Sb_5. Further work is needed to understand the nature of high-pressure phases in AV_3Sb_5, as well as clarify how they are related to the second superconducting dome.

In conclusion, we have systematically studied the electrical resistance of RbV_3Sb_5 by applying hydrostatic pressure via a liquid pressure medium, revealing the presence of two superconducting domes and distinct features in the normal state transport associated with the second dome, similar to KV_3Sb_5. In both systems, the shape of the first superconducting dome is

highly asymmetric, with maximal T_c near the border of the ambient pressure charge order. With increasing pressure, anomalies in dR/dT near $T^* \sim 220$ K appear at the edge of the first superconducting dome and persist across the second dome. The suppression of superconductivity in the second superconducting dome is associated with significant changes in the normal state transport, which can be attributed to a high-pressure phase. The commonality of a second superconducting dome at high pressures and behaviors in the normal state resistance for both RbV_3Sb_5 and KV_3Sb_5 suggests a link between these phenomena.

Acknowledgments

This work was supported by the National Key R&D Program of China (Grant Nos. 2017YFA0303100 and 2016YFA0300202), the Key R&D Program of Zhejiang Province, China (Grant No. 2021C01002), the National Natural Science Foundation of China (Grant Nos. 11974306 and 12034017), and the Fundamental Research Funds for the Central Universities of China. S.D.W. and B.R.O. gratefully acknowledge support via the UC Santa Barbara NSF Quantum Foundry funded via the Q-AMASE-i program under award DMR-1906325. B.R.O. also acknowledges support from the California NanoSystems Institute through the Elings fellowship program.

References

[1] Ortiz B R, Gomes L C, Morey J R, Winiarski M, Bordelon M, Mangum J S, Oswald I W H, Rodriguez-Rivera J A, Neilson J R, Wilson S D, Ertekin E, McQueen T M and Toberer E S 2019 *Phys. Rev. Mater.* **3** 094407

[2] Ortiz B R, Teicher S M, Hu Y, Zuo J L, Sarte P M, Schueller E C, Abeykoon A M, Krogstad M J, Rosenkranz S, Osborn R, Seshadri R, Balents L, He J and Wilson S D 2020 *Phys. Rev. Lett.* **125** 247002

[3] Yin Q, Tu Z, Gong C, Fu Y, Yan S and Lei H 2021 *Chin. Phys. Lett.* **38** 037403

[4] Ortiz B R, Sarte P M, Kenney E M, Graf M J, Teicher S M L, Seshadri R and Wilson S D 2021 *Phys. Rev. Mater.* **5** 034801

[5] Wang Y, Yang S, Sivakumar P K, Ortiz B R, Teicher S M L, Wu H, Srivastava A K, Garg C, Liu D, Parkin S S P, Toberer E S, McQueen T, Wilson S D and Ali M N 2020 Preprint arXiv: 2012.05898

[6] Liang Z, Hou X, Zhang F, Ma W, Wu P, Zhang Z, Yu F, Ying J J, Jiang K, Shan L, Wang Z and Chen X H 2021 *Phys. Rev. X* **11** 031026

[7] Yang S Y, Wang Y, Ortiz B R, Liu D, Gayles J, Derunova E, Gonzalez-Hernandez R, Šmejkal L, Chen Y, Parkin S S P, Wilson S D, Toberer E S, McQueen T and Ali M N 2020 *Science Advances* **6** eabb6003

[8] Yu F H, Wu T, Wang Z Y, Lei B, Zhuo W Z, Ying J J and Chen X H 2021 *Phys. Rev. B* **104** L041103

[9] Kenney E M, Ortiz B R, Wang C, Wilson S D and Graf M J 2021 *J. Phys.: Condens. Matter* **33** 235801

[10] Jiang Y X, Yin J X, Denner M M, Shumiya N, Ortiz B R, Xu G, Guguchia Z, He J, Hossain M S, Liu X, Ruff J, Kautzsch L, Zhang S S, Chang G, Belopolski I, Zhang Q, Cochran T A, Multer D, Litskevich M, Cheng Z J, Yang X P, Wang Z, Thomale R, Neupert T, Wilson S D and Hasan M Z 2021 *Nat. Mater.* **20** 1353

[11] Feng X, Jiang K, Wang Z and Hu J 2021 *Science Bulletin* **66** 1384

[12] Setty C, Hu H, Chen L and Si Q 2021 arXiv: 2105.15204

[13] Lin Y P and Nandkishore R M 2021 arXiv: 2107.09050

[14] Duan W, Nie Z, Luo S, Yu F, Ortiz B R, Yin L, Su H, Du F, Wang A, Chen Y, Lu X, Ying J, Wilson S D, Chen X, Song Y and Yuan H 2021 *Sci. China-Phys. Mech. Astron.* **64** 107462

[15] Mu C, Yin Q, Tu Z, Gong C, Lei H, Li Z and Luo J 2021 *Chin. Phys. Lett.* **38** 077402

[16] Xu H S, Yan Y J, Yin R, Xia W, Fang S, Chen Z, Li Y, Yang W, Guo Y and Feng D L 2021 *Phys. Rev. Lett.* **127** 187004

[17] Xiang Y, Li Q, Li Y, Xie W, Yang H, Wang Z, Yao Y and Wen H H 2021 *Nat. Commun.* **12** 6727

[18] Zhao C C, Wang L S, Xia W, Yin Q W, Ni J M, Huang Y Y, Tu C P, Tao Z C, Tu Z J, Gong C S, Lei H C, Guo Y F, Yang X F and Li S Y 2021 Preprint arXiv: 2102.08356

[19] Yu F H, Ma D H, Zhuo W Z, Liu S Q, Wen X K, Lei B, Ying J J and Chen X H 2021 *Nat. Commun.* **12** 3645

[20] Chen K, Wang N, Yin Q, Gu Y, Jiang K, Tu Z, Gong C, Uwatoko Y, Sun J, Lei H, Hu J and Cheng J G 2021 *Phys. Rev. Lett.* **126** 247001

[21] Du F, Luo S, Ortiz B R, Chen Y, Duan W, Zhang D, Lu X, Wilson S D, Song Y and Yuan H 2021 *Phys. Rev. B* **103** l220504

[22] Chen X, Zhan X, Wang X, Deng J, Liu X B, Chen X, Guo J G and Chen X 2021 *Chin. Phys. Lett.* **38** 057402

[23] Zhang Z, Chen Z, Zhou Y, Yuan Y, Wang S, Wang J, Yang H, An C, Zhang L, Zhu X, Zhou Y, Chen X, Zhou J and Yang Z 2021 *Phys. Rev. B* **103** 224513

[24] Zhu C C, Yang X F, Xia W, Yin Q W, Wang L S, Zhao C C, Dai D Z, Tu C P, Song B Q, Tao Z C, Tu Z J, Gong C S, Lei H C, Guo Y F and Li S Y 2021 Preprint arXiv: 2104.14487

[25] Yin L, Zhang D, Chen C, Ye G, Yu F, Ortiz B R, Luo S, Duan W, Su H, Ying J, Wilson S D, Chen X, Yuan H, Song Y and Lu X 2021 *Phys. Rev. B* **104** 174507

[26] Wang N N, Chen K Y, Yin Q W, Ma Y N N, Pan B Y, Yang X, Ji X Y, Wu S L, Shan P F, Xu S X, Tu Z J, Gong C S, Liu G T, Li G, Uwatoko Y, Dong X L, Lei H C, Sun J P and Cheng J G 2021 *Phys. Rev. Research* **3** 043018

[27] Wang W S, Li Z Z, Xiang Y Y and Wang Q H 2013 *Phys. Rev. B* **87** 115135

[28] Isakov S V, Wessel S, Melko R G, Sengupta K and Kim Y B 2006 *Phys. Rev. Lett.* **97** 147202

[29] Guo H M and Franz M 2009 *Phys. Rev. B* **80** 113102

[30] Kiesel M L, Platt C and Thomale R 2013 *Phys. Rev. Lett.* **110** 126405

[31] Wen J, Rüegg A, Wang C C J and Fiete G A 2010 *Phys. Rev. B* **82** 075125

[32] Zhang J F, Liu K and Lu Z Y 2021 *Phys. Rev. B* **104** 195130

[33] Tsirlin A A, Fertey P, Ortiz B R, Klis B, Merkl V, Dressel M, Wilson S D and Uykur E 2021 arXiv: 2105.01397 (Preprint)

[34] Lee S, Collini J, Sun S X L, Mitrano M, Guo X, Eckberg C, Paglione J, Fradkin E and Abbamonte P 2021 *Phys. Rev. Lett.* **127** 027602

[35] Werthamer N R, Helfand E and Hohenberg P C 1966 *Phys. Rev.* **147** 295